Open Access

Baghdad Science Journal **Vol.16 (4) Supplement 2019**

DOI: http://dx.doi.org/10.21123/bsj.2019.16.4(Suppl.).1093

Compact MIMO Slots Antenna Design with Different Bands and High Isolation for 5G Smartphone Applications

A.M. Ibrahim * ***I.M. Ibrahim*** ***N. A. shairi***

Received 2/7/2019, Accepted 2/12/2019, Published 18/12/2019

This work is licensed under a Creative Commons Attribution 4.0 International License.

Abstract:

In this paper, two elements of the multi-input multi-output (MIMO) antenna had been used to study the five (3.1-3.55GHz and 3.7-4.2GHz), (3.4-4.7 GHz), (3.4-3.8GHz) and (3.6-4.2GHz) 5G bands of smartphone applications that is to be introduced to the respective US, Korea, (Europe and China) and Japan markets. With a proposed dimension of 26 × 46 × 0.8 mm^3, the medium-structured and small-sized MIMO antenna was not only found to have demonstrated a high degree of isolation and efficiency, it had also exhibited a lower level of envelope correlation coefficient and return loss, which are well-suited for the 5G bands application. From the fabrication of an inexpensive FR4 substrate with a 0.8 mm thickness level, a loss tangent of 0.035 and a dielectric constant of 4.3, the proposed MIMO antennas that had been simulated under the five different band coverage were discovered to have demonstrated a respective isolation level of about 14dB, 12dB, 21.5dB, 19dB and 20dB under a -10dB impendence bandwidth. In the measurement and fabrication outcomes that were derived from the use of the prototype MIMO in the (3.4-3.8) band of the Europe and Chinese markets, the proposed MIMO was thus found to have produced a better performance in terms of efficiency, isolation, and envelope correlation coefficient (ECC).

Key words: 5G bands, Envelope correlation coefficient, Isolation, MIMO antenna.

Introduction:

The endless concern on the high data demand level and channel bandwidth in the contemporary wireless system was found to have prompted the development of the numerous integrated single-input multiple-output and multiple-input multiple-output antennas of a client's equipment. For this reason, the need to constantly improve the performance of the multi-input multi-output antenna (MIMO) design had not only spurred the various studies on polarization diversity, gain value, bandwidth level, coupling reduction among the inter-elements and those of channel capacity, it had also allowed the designers to develop a more modern system network from the much improved multi-band resonance and impedance bandwidth.

[1] Centre for Telecommunication Research and Innovation (CeTRI), Fakulti Kejuruteraan Elektronik dan Kejuruteraan Komputer, Universiti Teknikal Malaysia Melaka (UTeM), Hang Tuah Jaya, 76100 Durian Tunggal, Melaka, Malaysia.

*Corresponding author: ayman971972@gmail.com

Since these designs would also require reducing the size of the multiple-element antenna (MEA) for them to be fitted and matched according to the users' robust applications and for supporting the equipment's multi-band coverage area, the development of a radiation diversity would then be helpful for reducing the correlation factor as well as improving the performance level of the MIMO system. Given that the MIMO wireless systems has the capacity to surge without requiring a rise in its spectrum or transmission power, the main challenge would then be to create an antennaed MIMO array that reduces the mutual coupling (1,2) from the introduction of a sixteen, twelve, ten and eight multi-element combination in its multi-input multi-output arrays(3–6).

In (4), although a group of sixteen antennas was analyzed at a developed channel capacity of about 70bps /Hz, the 10 dB isolation was only supported by just three neutralization lines, while the design in (7) had only utilised four small two-antennaed building block structures in creating an eight-antennaed MIMO system.

Table 1. Comparisons of Previously Published Literature

Ref.	DM	BW (GHz)	Size (mm^2), material, number of port	Eff. (%)	ECC	Iso. (dB)	Weak Point
(3)	-	(3.4 - 3.8), (-6 dB)	140×70, FR4 substrate, (10- elements)	(40 - 60)	0.1	-10	Not mentioned decoupling method, low isolation value and return loss start from -6 dB
(8)	-	(3.4 - 3.6), (-6 dB)	120 × 60, Rogers R04003c, (8 - elements)	(59 - 72)	-	-	Not mentioned decoupling method, medium structure, not mentioned isolation value, not mentioned ECC value, expensive material, and return loss start from -6 dB.
(9)	-	(2.55-2.65), (-10 dB)	136 × 68, FR4 substrate, (8 - elements)	(48 - 63)	0.15	-12	Not mentioned decoupling method, high ECC value, low isolation value.
(10)	-	(3.4-3.6)-(5.15-5.92), (-6 dB)	120 × 65, FR4 substrate, (8- elements)	50	0.1	-12	Not mentioned decoupling method, medium structure, low efficiency, high ECC value, low isolation value and return loss start from -6 dB.
(11)	-	(3.45-3.55), (-6 dB)	74 × 74, Rogers, RO4350b, Three layers, (24- elements)	64	0.119	-15	Not mentioned decoupling method, very complex structure, expensive material and return loss start from -6 dB.
(12)	DN	(6-9), (-10 dB)	40 × 40, Not mentioned, (2 - elements)	-	-	−15	Very complex structure, not mentioned material, Not mentioned ECC value and Not mentioned efficiency value .
(13)	DN	(0.7- 0. 96) and (1.7–2.17), (-10 dB)	150 × 80, FR4 substrate, (2 - elements)	(40 - 57)	-	–10 and –15	Large size , low efficiency, Not mentioned ECC value and Not mentioned efficiency value
(14)	MM	(1-2) GHz (-10 dB)	110 × 80, Not mentioned, (2 - elements)	-	-	–25	complex structure, Large size, Not mentioned ECC value and Not mentioned efficiency value.
(4)	NL	(3.4 - 3.6), (-6 dB)	150*75 FR4 substrate, (8 and 16 elements)	(40 - 60)	0.32	-10	high ECC value, low isolation value and return loss start from -6 dB
(15)	NL	(1.66-2.84), (-10 dB)	115×60 FR4 substrate, (2 - elements)	(63 – 65)	0.3	-15	Medium structure, large size and high ECC value.
(16)	NL	(3.4 - 3.8) (-6 dB)	140 × 70, FR4 substrate, (10- elements)	(40 - 57)	0.1	-10	Low efficiency, Low isolation value and return loss start from -6 dB.
(17)	NL	(3.1 – 12), (-6 dB)	40 × 80, FR4 substrate, (2 - elements)	-	-	-11	Medium structure, Large size ,Not mentioned ECC value , Not mentioned efficiency value and low isolation.
(18)	NL	(3.4 - 3.6), (-10 dB)	140 × 70, FR4 substrate (8 - elements)	(62 - 78)	02	-10	high ECC value and low isolation.
(19)	NL	(3.4 - 3.6) (-6 dB)	150 × 57, FR4 substrate, (16 - elements)	(30 - 53)	0.3	-10	Medium structure, low efficiency, high ECC value, low isolation and return loss start from -6 dB
(20)	NL	(2.62-2.69) and (5.15-5.92), (-10 dB)	140 × 70, FR4 substrate, (6 - elements)	60	0.05	-10	High size, low isolation and return loss start from -6 dB.
(21)	NL	(3.4 - 3.6), (-6 dB)	150 × 75, FR4 substrate, (8 - elements)	(40 - 52)	0.15	-10	Medium structure, high ECC, low isolation, low efficiency and return loss start from -6 dB.
(22)	NL	(3.4 - 3.8) and (5.15-5.92),	150 × 80, FR4 substrate, (12- elements)	(41-80), (47-79)	0.15 and 0.1	-10	Medium structure, high ECC, low isolation and return loss start from -6 dB.

		(-6 dB)					
(23)	DGS	(3.3 - 3.6), (-10 dB)	72 × 72, FR4 substrate, (4 - elements)	78	0.3	-28.8	Very complex structure, high ECC, low, large size and return loss start from -6 dB.
(24)	DGS	(4.25 -4.65) and (3.25 -3.4), (-10 dB)	102 × 80, FR4 substrate, (2 - elements)	-	0.15	–18 and –21	Large size, high ECC, and not mentioned efficiency.
(25)	DGS	(0.75-0.96) (1.38 - 2.7), (-10 dB)	52×77.5 FR4 substrate, (2 -elements)	(40 - 67)	0.5	-15	Complex structure, large size, high ECC and low isolation.
(26)	DGS	(2.4 - 2.48) and (5.15-5.82) (-10 dB)	25×24 FR4 substrate, (2 - elements)	-	0.04	-20	Not mentioned efficiency.
(27)	PB	(1.7 - 2.28), (-10 dB)	112×100 FR4 substrate, (3 - elements)	-	-	20	Complex structure, large size, not mentioned ECC and Not mentioned efficiency.
(28)	PD	(3.45-3.59), (-6 dB)	160×68.8 FR4 substrate, (8 - elements)	-	0.08	-15	Not mentioned efficiency.
(1)	PD	(3.5-5.7) and (5.8 – 4.3), (-10 dB)	36×36, Not mentioned, (4 - elements)	(63-65)	0.15	-15	Complex structure, large size, not mentioned ECC, not mentioned efficiency and return loss start from -6 dB.
(6)	PO	(3.4 - 3.6), (-6 dB)	150×75 FR4 substrate, (12 - elements)	50	0.2	-12.5	Medium structure, low ECC, low isolation, low efficiency and return loss start from -6 dB.
(5)	PO	(2.55-2.65), (-6 dB)	136×68 FR4 substrate, (8 - elements)	(40 – 60)	0.15	-12.5	Low ECC, low isolation, and return loss start from -6 dB.
(29)	Hyper (NL and DGS)	(3.3 - 3.6), (-6 dB)	124×74, FR4 substrate, (8 - element)	40	0.15	-15	Low ECC, low efficiency and return loss start from -6 dB.
(30)	Hyper (NL and DGS)	(3.1-3.55) - (4.4-4.99)/ (3.4-3.6) - (5.1-5.85, (-10 dB)	31×31, FR4 substrate, (2 - element)	(60-70) - (52-64) Or (66-70)- (35-52)	0.01, 0.005 Or 0.02, 0.005	-10, -19, -12 and -19	Medium structure and low efficiency.
This study	Hyper (NL and DGS)	(3.1- 3.55)/ (3.4 - 4.7)/ (3.4 - 3.8)/ (3.6 - 4.2)/ Or (3.7 - 4.2), (-10 dB)	26 × 46, FR4 substrate, (2 - elements)	(64 - 72), (66 - 85), (70 - 81), (78 - 90) or (78 - 87)	0.008 0.008 0.002 0.007 or 0.003	-14 -12 -21.5 -19 or -20	Medium structure.

DM= Decoupling Method; BW=Bandwidth; eff.=efficiency; ECC=Envelop Correlation Cofficient; Iso.=; NL= Neutralization Lines; DGS= Defected Ground Structures; DN= Decoupling Network; MM= Meta-materials; PB= Parasitic Branches; PD= Pattern Diversity; PO= Polarization Orthogonal.

Apart from the orthogonally polarized technique(5,6,23), the use of the eight elements was also found to have enhanced the channel capacity with the three existing neutralization lines creating a secured MIMO dual antenna isolation (15,30). In (31), a MIMO monopole antenna with a ground branch decoupling structure of less than 0.01 ECC, low mutual coupling and more than 20dB of high isolation was also proposed. Covering a band of 2.2-2.48GHz, this dual polarized MIMO antenna system of four orthogonal thin copper dipoles (23) was also discovered to have been popularly used in the high-order decoupling modes (32). The MIMO antenna elements that had been placed in the constant null-amplitude field points too were found

to have given rise to an enhanced isolation as a result of the respective usage from the decoupling network-based method (33) on a pair of narrow and wide slots as well as the two decoupling devices with an inverted T-shaped etched slot and a meandering resonant branch for the lower and higher bands. Besides the use of a compact split-ring resonator structure (SRR) and a planar spiral line (PSL) in the resonance structure method(34), a high level of isolation was also observed by changing the electrical length of the radiators through the pattern diversity technique (1, 29) and decreasing the mutual coupling of the ordered pairs with the introduction of the orthogonal mode (35), although the latter condition can also be achieved by implementing the decoupling network (33), pattern diversity technique (1,28), a resonance structure (34) and those of defected ground structures (25,26).

Since the focus on smart device miniaturization would require a lesser space for antenna design and consequently, affecting the close association between those of isolations and bandwidth in the MIMO antenna system, this paper had therefore attempted to solve the above mentioned issues with a high isolation that is printed on two element arrays operating at a 3.325GHz, 3.95GHz, 4.05GHz, 3.6GHz, 3.9GHz and the (3.1-3.55GHz and 3.7-4.2GHz), (3.4-4.7 GHz), (3.4-3.8GHz) and (3.6-4.2GHz) bands that are to be used in the US, Korea, (Europe and China) and Japan markets. With that in mind, the MIMO antenna that had consisted of two elements was thus placed symmetrically on the frame with the patch slots and the grounded neutralization lines of the hybrid decoupling structures generating the high isolation level.

By combining the neutralization line structure with the ground slots, the isolations from the mobile-phone antenna prototype that was measured and fabricated at the centre frequency band of 3.6GHz for (3.4-3.8) were then further enhanced with a centre frequency of 3.6GHz to 21.5 dB, while the 0.002 ECC that had existed between the two-elements was found to have provided a favourable performance as shown by its field radiation characteristic and the minimum efficiency for antenna elements, which had exceeded 70% of the operating band. As shown by the comparison of the decoupling designs in Table1, the small antenna-designed of the proposed decoupling design as compared to the other two element MIMO designs was not only found to have exhibited a higher level of isolation and efficiency, but also the ability for accomodating to different bands as a result of its lower correlation coefficient from the hybrid decoupling structures.

Design of Antenna Elements

The proposed design of the two-port MIMO antenna, which had consisted of two closely spaced monopoles of 2mm that is printed on a 26 × 46 mm FR 4 substrate with a 4.3 dielectric constant, 0.035 of copper thickness and a 0.8 mm of the FR4 substrate thickness is thus shown in Fig.1.

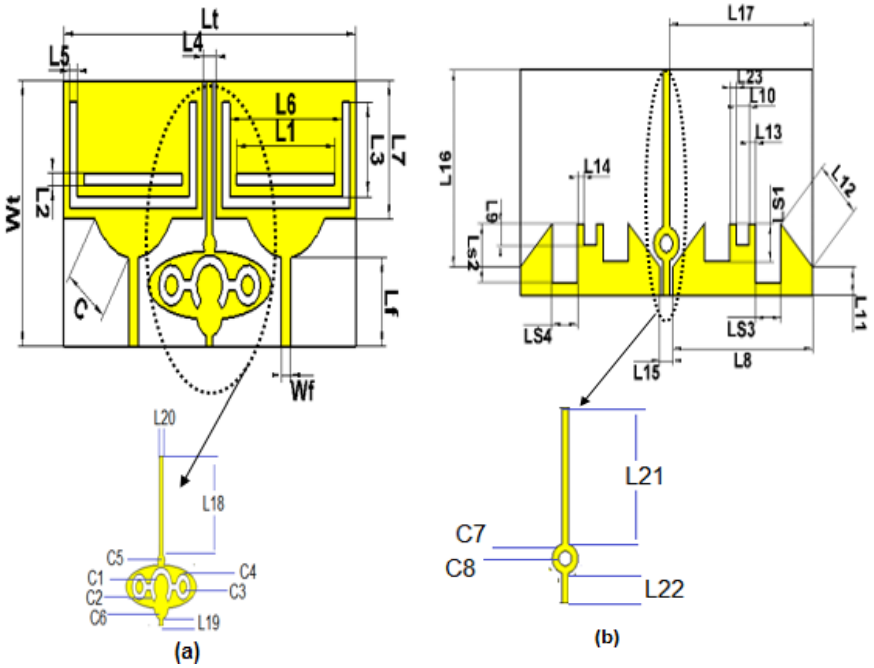

Figure 1. The Proposed Design Geometry of the MIMO Antenna (A) Front View (B) Back View

As depicted in Fig.1, the ground plane of this design had utilised both the notch structure as well as a twofold U-shaped incision with the U- and L-shaped inserts in the patch monopole. The

impedance matching of the proposed antenna was also enhanced by cutting off a rectangular slot around the micro strip line of the ground plane that is located at the back of the substrate. The simulation is performed using computer simulation software (CST) (36–39).

In this design, since the notched function had been limited by the slot length, the relationship between the length of the slot and the frequency band notch can therefore be expressed as such:

$$f_{notch} = \frac{c}{2L_{slot}\sqrt{\in_{eff}}} \quad (1)$$

$$\in_{eff} = \frac{\in_r - 1}{2} \quad (2)$$

where f notch is the resonant frequency, U-slot is the length of the slot, c is the speed of the light and ∈r is the constant dielectric of the substrate (40). A summary of the parameter dimensions for the MIMO antenna array is thus shown in Table 2.

Table2. The MIMO Antenna Dimensions Parameters

Parameters	**L1**	**L2**	**L3**	**L4**	**L5**	**L6**
Dimensions (mm)	15.45	1.15	9.25	2	1.15	17.7
Parameters	**L7**	**L8**	**L9**	**L10**	**L11**	**L12**
Dimensions (mm)	13.5	22	2.5	2	3.3	7.07
Parameters	**L13**	**L14**	**L15**	**L16**	**L17**	**L18**
Dimensions (mm)	5	5	2	22.72	17.22	15.16
Parameters	**L19**	**L20**	**L21**	**L22**	**Lt**	**Lf**
Dimensions (mm)	1.35	1	18.06	4.06	46	8.69
Parameters	**Wt**	**Wf**	**hs**	**ht**	**C**	**R1**
Dimensions (mm)	26	1.47	0.8	0.035	6.55	9.7
Parameters	**R2**	**C1**	**C2**	**C3**	**C4**	**C5**
Dimensions (mm)	3.35	1	1.5	0.5	1	0.5
Parameters	**C6**	**C7**	**C8**	**LS3**	**LS4**	**L23**
Dimensions (mm)	1	1	0.5	4	4	1

Decoupling Structure:

The geometric structure of the copper line with a circular ground plane that is depicted in Fig.1 had not only composed of a vertical centre piece with two split up antennas and a neutralization line that had been inserted between the two antenna monopoles of the patch antenna, but also the use of slots for changing the bandwidth.

For this reason, the 5G band decoupling had been successfully achieved from the two patch and ground metal stripped antennas as well as from the elliptical metal disc from the neutralization line, where it had provided the possible decoupling current paths with different lengths and overriding those on the ground plane.

The two circular slots that were connected via an arch and etched on the elliptical metal disc of the neutralization line were also found to have greatly reduced the decoupling frequencies to a value that is lesser than 5 GHz.

It is also important to note that the distance between the top of the ground plane and the elliptical disc (M1) had been that of 15.16 mm, while the respective distances from the bottom of the ground plane to the centre of the elliptical disc (on the neutralization line) (M2), the metal arch disc (M3), circular metal slot (M4) and circular slot (M5) had been of 15.16 mm, 6.59 mm, 8.12 mm and 8.12 mm.

Simulation Results:

The effects of the (LS1) and (LS2) slot widths on the frequency response and bandwidth that were explained from a parametric study had also shown the slot widths as having a high sensitivity level towards the MIMO antenna design, since the increase or decrease in the (LS1) and (LS2) ground plane slots width values were found to have induced a change in the centre resonant frequency of the design bandwidth. The isolations of the different adjacent antennas that had resulted from the changes of the (LS1) and (LS2) slot widths are thus illustrated in Fig.2.

A summary of the centre frequency, bandwidth, ECC, isolation and the efficiency values from the change of the (LS1) and (LS2) slot widths is also shown in Table 3.

Table 3. Effects on Bandwidth and Isolation from the LS1 and LS2 Slots Width

LS1 (mm)	LS2 (mm)	centre (GHz)	B.W (GHz)	ECC	Isolation dB	Eff. dB
4.8	7.8	3.325	3.1-3.55	0.008	-14	64-72
8.3	2.8	4.05	3.4-4.7	0.008	-12	66-85
6.8	6.8	3.6	3.4-3.8	0.002	-21.5	70-81
1.8	4.8	3.9	3.6-4.2	0.007	-19	78-90
6.8	4.8	3.95	3.7-4.2	0.003	-20	78-87

and LS2 ground antenna slot lengths since the various LS1 and LS2 lengths that were used on the various bands (3.1-3.55GHz), (3.4-4.7 GHz), (3.4-3.8GHz), (3.6-4.2GHz) or (3.7-4.2GHz) for the US, Korea, Europe, China and Japan markets were discovered to have resulted a respective high isolation of about 14 dB, 12 dB, 21.5 dB, 19dB or 20 dB. Apart from the above, the proposed antenna too was seen as providing a higher level of efficiency such as those of (64-72), (66-85), (70-81), (78-90) and (78-87) on the respective (3.1-3.55GHz), (3.4-4.7 GHz), (3.4-3.8GHz), (3.6-4.2GHz) or (3.7-4.2GHz) operation bands.

To illustrate the effect of the bending structures on the production of operating bands, the proposed antenna was then simulated with the various LS1 and LS2 values, where the simulated S11, S22, S12 and S21 outcomes are shown in Fig. 2 (a), (b), (c), (d) and (e). Since the use of antenna 1 in Fig. 1 had been symmetrical to that of antenna 2, the results from the proposed MIMO antennas were found to have exhibited an equal return loss values (S11 and S22) as well as those of isolation (S12 and S21). The difference in the results of the proposed MIMO antenna that was used in the 5G application had also implied the possible influence of the LS1

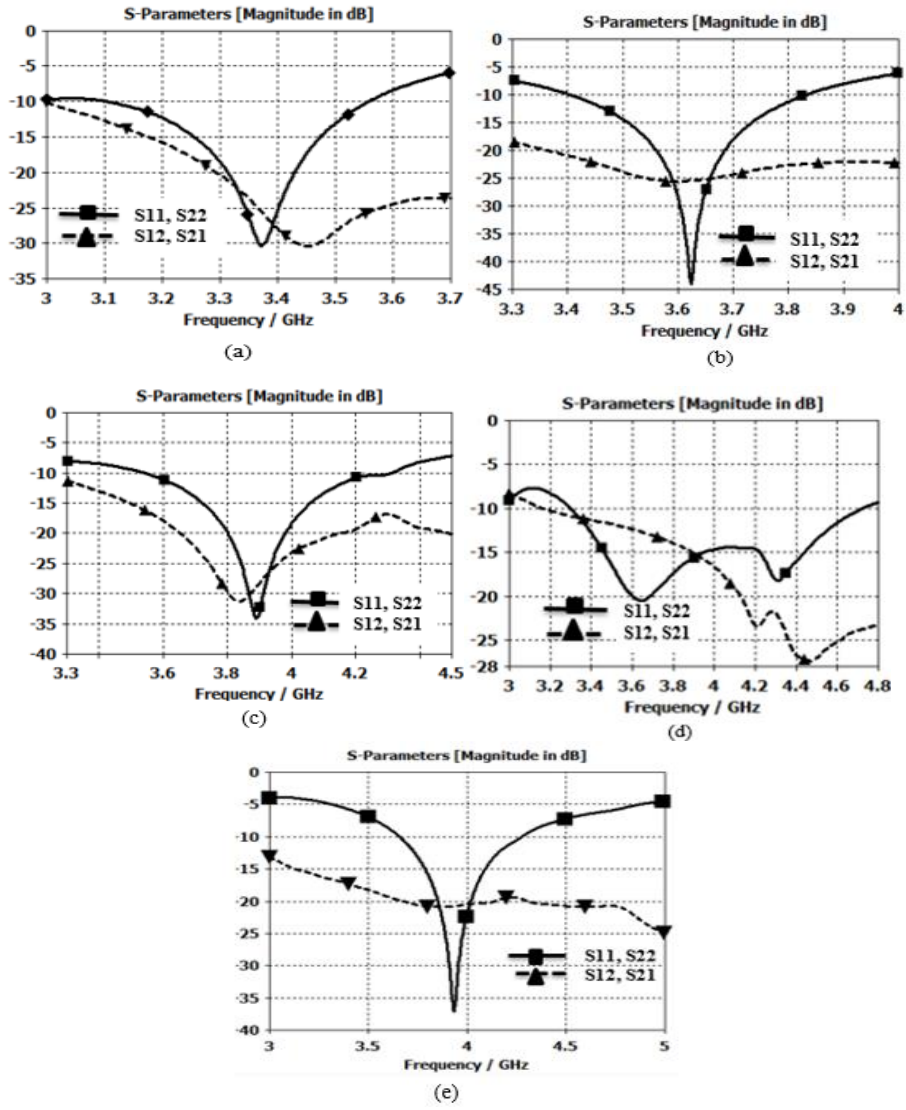

Figure 2. Simulated Reflection Coefficients and Transmission Coefficients of the Two Antennas with LS1 and LS2 Slots. (a) S- Parameters of the (3.1-3.55) GHz Band, (b) S- Parameters of the (3.4-3.8) GHz Band, (c) S- Parameters of the (3.6-4.2) GHz Band, (d) S- Parameters of the (3.4-4.7) GHz Band, and (e) S- Parameters of the (3.7-4.2) GHz Band.

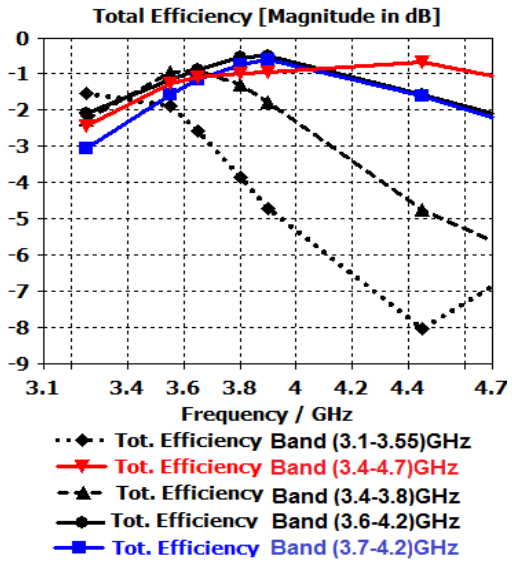

Figure 3. Simulated Antenna Total Efficiency

Besides showing the two antenna ports of the MIMO antenna for the (3.4-3.8) band as having a distributed surface current of 3.6 GHz, the diagram in Fig.3 had also successfully demonstrated the antenna as having a different set of feeding ports as well as the opposing current densities caused by the diverse polarization levels. The ground plane of the MIMO antenna as depicted in Fig.4 had also revealed its surface currents as being mainly distributed around the slot areas.

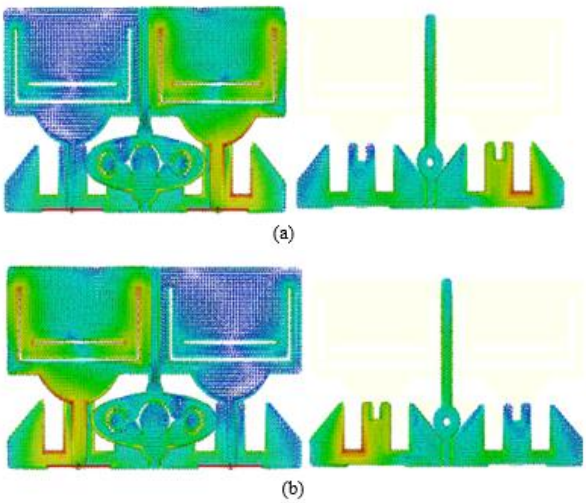

Figure 4. Simulated current densities at 3.6 GHz central frequency of the (3.4-3.8) band
(a) current densities of antenna1 and (b) current densities antenna2.

Measured Results:

By fabricating a mobile antenna prototype for the (3.4-3.8) band with a 3.6 GHz central frequency from an inexpensive FR4 dielectric with an overall dimension of 26 × 46 × 0.8 mm^3 as those shown in Fig.5, the simulated and measured reflection and transmission coefficients that were demonstrated by the two representative antennas (antenna1 and antenna2) in Fig. 6 had therefore implied the two as having a similar level of performance.

Figure 5. A photograph of the two fabricated antennas.

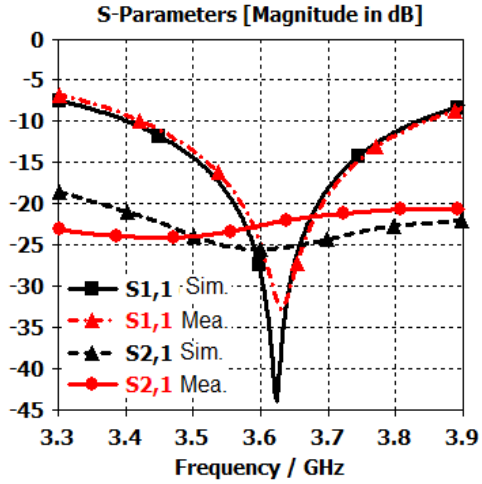

Figure 6. Simulated and Measured (A) Transmission Coefficients and Reflection Coefficients of the two antennas.

As depicted in the above figure, the (LS1 and LS2) slots from the ground plane were found to have given rise to S-parameters with a low mutual coupling characteristic and a -10dB impedance bandwidth with the (3.4-3.8GHz) operating band coverage. While the measured results of the S12 and S21 transmission parameters had indicated a good isolation property with less than -19 dB in the operating range and an isolation of less than -20 dB in the simulated outcome, some deviations from the measurement results were still being observed as a result of the errors that had stemmed from the feeding and fabrication processes.

Since the correct operation of the multi-input multi-output antennas can be safeguarded from the incorporation of an envelope correlation coefficient (ECC) in the MIMO antennas, this parameter can therefore be calculated from the S-parameters by using the following method:

$$ECC = \frac{\left|S_{11}^{*}S_{12} + S_{21}^{*}S_{22}\right|^2}{(1-\left|S_{11}\right|^2-\left|S_{21}\right|^2)(1-\left|S_{22}\right|^2-\left|S_{12}\right|^2)} \qquad (3)$$

From the measured and simulated S-parameters envelope correlation coefficient results of the proposed mobile phone antenna that were calculated in Fig.7, it was obvious that the calculated ECC results had been within the low mutual coupling of the (3.4-3.8GHz) band with a frequency of 3.6 GHz hence, confirming the existence of a high isolation between the two adjacent antenna elements from the use of the proposed MIMO antenna.

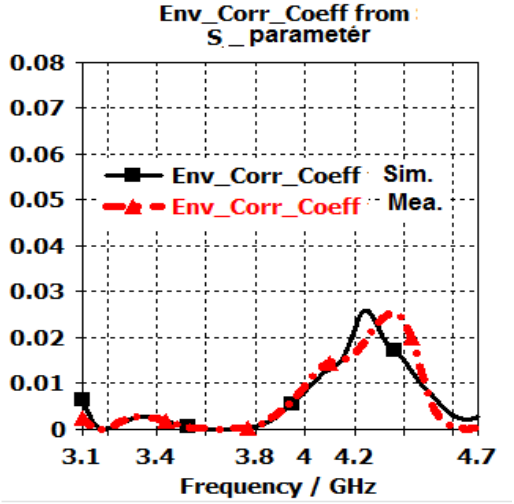

Figure 7. Simulated and Envelope correlation coefficient (ECC) of the two antennas

Conclusion:

A compact sized 5G MIMO antenna was designed and implemented at low cost. The results show good RL for the centre frequency in order for the antenna to be used for used the five (3.1-3.55 GHz and 3.7-4.2 GHz), (3.4-4.7 GHz), (3.4-3.8 GHz) and (3.6-4.2 GHz) 5G bands of smartphone applications. By controlling the different bands from the two slots in the ground plane, the different centre frequencies, S-parameters, efficiency levels and ECC results that had been exhibited by the antenna elements were thus studied and analysed. From the results of the analysis, the prototype of a mobile-phone antenna that was fabricated and measured at a 3.6GHz centre frequency for the (3.4-3.8) band was not only found to have demonstrated a respective simulated and measured isolation results of (-21.5) dB and (-19) dB, but had also provided good characteristics and meeting the future usage requirements of mobile phones.

Acknowledgment

The authors would like to thank universiti Teknikal Malaysia Melaka (UTeM) and Ministry of Higher Education for sponsoring this work under research grants PJP/2017/FKEKK/HI10/S01529.

Conflicts of Interest: None.

References:

1. Boukarkar A, Lin XQ, Jiang Y, Nie LY, Mei P, Yu YQ. A miniaturized extremely close-spaced four-element dual-band MIMO antenna system with polarization and pattern diversity. IEEE Antennas Wirel Propag Lett. 2018;17(1):134–7.
2. Qian K, Zhao L, Wu KL. An LTCC Coupled Resonator Decoupling Network for Two Antennas. IEEE Trans Microw Theory Tech. 2015;63(10):3199–207.
3. Lu K-LW , JY. 3.6-GHz 10-antenna array for MIMO operation in the smartphone. Microw Opt Technol Lett. 2015;57(7):1699–704.
4. Wong KL, Lu JY, Chen LY, Li WY, Ban YL. 8-antenna and 16-antenna arrays using the quad-antenna linear array as a building block for the 3.5-GHz LTE MIMO operation in the smartphone. Microwave and Optical Technology Letters. 2016 Jan;58(1):174-81.
5. Li M-Y, Xu Z-Q, Ban Y-L, Sim C-Y-D, Yu Z-F. Eight-port orthogonally dual-polarised MIMO antennas using loop structures for 5G smartphone. IET Microwaves, Antennas Propag [Internet]. 2017;11(12):1810–6. Available from: https://digital-library.theiet.org/content/journals/10.1049/iet-map.2017.0230
6. Li MY, Ban YL, Xu ZQ, Guo J, Yu ZF. Tri-Polarized 12-Antenna MIMO Array for Future 5G Smartphone Applications. IEEE Access. 2018;6:6160–70.
7. Wong KL, Tsai CY, Lu JY. Two Asymmetrically Mirrored Gap-Coupled Loop Antennas as a Compact Building Block for Eight-Antenna MIMO Array in the Future Smartphone. IEEE Trans Antennas Propag. 2017;65(4):1765–78.
8. Report F, Mushiake Y, Guo L, Wang S, Gao Y, Wang Z, et al. EIGHT-ELEMENT ANTENNA ARRAY FOR DIVERSITY AND MIMO MOBILE TERMI- NAL IN LTE 3500 MHz BAND. 2014;56(6):1323–7.
9. Li M, Ban Y, Xu Z, Wu G, Sim C, Member S, et al. Eight-Port Orthogonally Dual-Polarized Antenna Array for 5G Smartphone Applications. IEEE Trans Antennas Propag. 2016;64(9):3820–30.
10. Zou H, Li Y. Design of 8 × 8 dual-band MIMO antenna array for 5G smartphone applications. Int J RF Microw Comput Eng. 2018;2500(March):1–12.
11. Al-tarifi MA, Sharawi MS, Shamim A. Massive MIMO antenna system for 5G base stations with directive ports and switched beamsteering capabilities. 2018;1709–18.
12. Xia R, Qu S, Member S, Li P, Jiang Q, Nie Z. An Efficient Decoupling Feeding Network for Microstrip Antenna Array. IEEE Antennas Wirel Propag Lett. 2014;1225(c):1–4.
13. Chen W, Lin H. LTE700 / WWAN MIMO Antenna System Integrated with Decoupling Structure for Isolation Improvement. IEEE Antennas Propag Soc Int Symp. 2014;689–90.
14. Ren Y, Ding J, Guo C, Qu Y, Song Y. A Wideband Dual-Polarized Printed Antenna Based on Complementary Split-Ring Resonators. IEEE Antennas Wirel Propag Lett. 2015;14:410–3.
15. Wang Y, Du Z. A wideband printed dual-antenna

with three neutralization lines for mobile terminals. IEEE Trans Antennas Propag. 2014;62(3):1495–500.
16. Rudish RM, Electron D, Volakis JL, Society P, Symposium I, Diego S, et al. 3 . 6-GHz 10-ANTENNA ARRAY FOR MIMO OPERATION IN THE. 2015;57(7):1699–705.
17. Yu Y, Liu X, Gu Z, Yi L. A Compact Printed Monopole Array with Neutralization Line for UWB Applications. 2016 IEEE Int Symp Antennas Propag. 2016;1779–80.
18. Ban Y, Li C, Sim C, Member S, Wu G. 4G / 5G Multiple Antennas for Future Multi-Mode Smartphone Applications. IEEE Access. 2016;3536(c).
19. Wong KL, Lu JY, Chen LY, Li WY, Ban YL. 8-antenna and 16-antenna arrays using the quad-antenna linear array as a building block for the 3.5-GHz LTE MIMO operation in the smartphone. Microwave and Optical Technology Letters. 2016 Jan;58(1):174-81.
20. Zou H, Li Y, Shen H, Wang H, Yang G. Design of 6 × 6 Dual-Band MIMO Antenna Array for 4 . 5G / 5G Smartphone Applications. Asia-Pacific Conf Antennas Propag. 2017;1–3.
21. Wong K, Tsai C, Member S, Lu J. Two Asymmetrically Mirrored Gap-Coupled Loop Antennas as a Compact Building Block for Eight-Antenna MIMO Array in the Future. IEEE Trans Antennas Propag >. 2017;(c):1–14.
22. Li Y, Sim C. 12-Port 5G Massive MIMO Antenna Array in Sub-6GHz Mobile Handset for LTE Bands 42 / 43 / 46 Applications. IEEE Access. 2018;6:344–54.
23. Huang H, Li X, Liu Y. 5G MIMO antenna based on vector synthetic mechanism. IEEE Antennas Wirel Propag Lett. 2018;17(6):1052–5.
24. Yu Y, Yi L, Liu X, Gu Z, Rizka NM. Dual-Frequency Two-Element Antenna Array with Suppressed Mutual Coupling. Int J Antennas Propag. 2015;2015.
25. Dong J, Yu X, Deng L. A Decoupled Multiband Dual-Antenna System for WWAN/LTE Smartphone Applications. IEEE Antennas Wirel Propag Lett. 2017;16(c):1528–32.
26. Deng J, Li J, Zhao L, Guo L. A Dual-Band Inverted-F MIMO Antenna with Enhanced Isolation for WLAN Applications. IEEE Antennas Wirel Propag Lett. 2017;16(c):2270–3.
27. Li Z, Du Z, Takahashi M, Saito K, Ito K. Reducing mutual coupling of MIMO antennas with parasitic elements for mobile terminals. IEEE Trans Antennas Propag. 2012;60(2 PART 1):473–81.
28. Ding CF, Zhang XY, Xue CD, Sim CYD. Novel Pattern-Diversity-Based Decoupling Method and Its Application to Multielement MIMO Antenna. IEEE Trans Antennas Propag. 2018;66(10):4976–85.
29. Jiang W, Liu B, Cui Y, Hu W. High-Isolation Eight-Element MIMO Array for 5G Smartphone Applications. IEEE Access. 2019;7:34104–12.
30. Ibrahim A.M, Ibrahim I.M, shair NA . Compact MIMO Slot Antenna of Dual-Band for LTE and 5G Applictaions. International Journal of Advanced Science and Technology. 2019;No 13(28):239-246.
31. XueMing Ling, RongLin Li. A Novel Dual-Band MIMO Antenna Array With Low Mutual Coupling for Portable Wireless Devices. IEEE Antennas Wirel Propag Lett. 2011;10:1039–42.
32. Prakash J, Roshan V, Natarajamani S. MIMO Antenna for mobile terminals with enhanced isolation in LTE band. 2017 Int Conf Adv Comput Commun Informatics, ICACCI 2017. 2017;2017-Janua:2231–4.
33. Zhao X, Yeo SP, Ong LC. Decoupling of Inverted-F Antennas with High-Order Modes of Ground Plane for 5G Mobile MIMO Platform. IEEE Trans Antennas Propag. 2018;66(9):4485–95.
34. Ding C, Li Q, Yang Y, Lei X, Wu G, Huang M, et al. A Compact Dual-Band MIMO Slot Antenna for WLAN Applications. 2018 IEEE Antennas Propag Soc Int Symp Usn Natl Radio Sci Meet APSURSI 2018 - Proc. 2018;461–2.
35. Xun JH, Shi LF, Liu WR, Liu GX, Chen S. Compact Dual-Band Decoupling Structure for Improving Mutual Coupling of Closely Placed PIFAs. IEEE Antennas Wirel Propag Lett. 2017;16(c):1985–9.
36. Sun L, Feng H, Li Y, Zhang Z. Compact 5G MIMO mobile phone antennas with tightly arranged orthogonal-mode pairs. IEEE Trans Antennas Propag. 2018;66(11):6364–9.
37. Ibrahim A.M, Ibrahim I.M, shair NA . A Compact Quad Bands-Notched Monopole antenna for Ultra-Wideband Wireless Communicatione. RELIGACION. 2019;No 17(4,julio):815–824.
38. Ibrahim A.M, Ibrahim I.M, shair NA . A Compact Sextuple Multi-Band Printed Monopole Antenna. Opcion. 2018;86(34):1448–1467.
39. Ibrahim A.M, Ibrahim I.M, shair NA . Design a Compact Wide Bandwidth of a printed Antenna using Defected Ground Structure. Jour of Adv Research in Dynamical & Control Systems.2019;11(02):1065-1076.
4o. Mewara HS, Jhanwar D, Sharma MM, Deegwal JK. A printed monopole ellipzoidal UWB antenna with four band rejection characteristics. AEU - Int J Electron Commun [Internet]. 2018;83:222–32.

تصميم هوائي متعدد المدخلات متعدد المخرجات ذو الفتحات مع نطاقات مختلفة وعزلة عالية لتطبيقات الهواتف الذكية للجيل الخامس

ايمن محمد إبراهيم **عمران محمد إبراهيم** **نور غزوان شاري**

مركز أبحاث الاتصالات والابتكار ((CeTRI)، كلية الإلكترونيات وهندسة الكمبيوتر ، جامعة مالاكا التقنية ((UTeM، هانغ تواه جايا ، 76100 دوريان سينجل ، ميلاكا ، ماليزيا.

الخلاصة:

في هذه الورقة ، تم استخدام عنصرين من هوائي متعدد المدخلات متعدد المخرجات (MIMO) لدراسة النطاقات ((3.1-3.55) - (3.7-4.2) - (3.4-4.7) - (3.4-3.8) - (3.6-4.2)) جيجا هيرتز لتطبيقات الجيل الخامس(G5) والمستخدمة في الهواتف الذكية التي سيتم طرحها في أسواق الولايات المتحدة وكوريا وأوروبا والصين واليابان. يبلغ حجم الهوائي المقترح 26 × 46 × 0.8 ملم مكعب، مع هيكل مناسب وصغير الحجم اضافة الى ذلك أظهر الهوائي المقترح عزلة وكفاءة عاليتين، كذلك اظهر مستوى منخفض لمعامل الارتباط المغلف (ECC) وعودة الخسارة، هذه المواصفات تتناسب تماما تطبيقات الجيل الخامس (5G). وقد تم تصنيع الهوائي المقترح من مادة FR4 الغيرمكلفة بمستوى سماكة 0.8 ملم، وشدة فقدان مقدارها 0.035 وثابت عازل قدره 4.3 ، اظهرت نتائج المحاكاة لهوائيات MIMO المقترحة التي تغطي النطاقات الخمسة المختلفة مستوى عزل عالي لكل منها حوالي 14 ديسيبل و 12 ديسيبل و 21.5 ديسيبل و 19 ديسيبل و 20 ديسيبل تحت عرض النطاق الترددي العائق -10 ديسيبل. ومن خلال التصنيع والقياس للنموذج الاولي لهوائي (MIMO) الذي يغطي النطاق (3.4-3.8) المستخدم في كل من أوروبا والصين، وجد أن الهوائي المقترح قد حقق أداء أفضل من حيث الكفاءة والعزلة ومعامل الارتباط المغلف(ECC).

الكلمات المفتاحية: نطاقات ترددات الجيل الخامس، معامل الارتباط المغلف، عزل الهوائيات، هوائي متعدد المخلات متعدد المخرجات.